Spin polarization by first-principles relativistic $\mathbf{k}\cdot\mathbf{p}$ theory: Application to the surface alloys $PbAg_2$ and $BiAg_2$

I. A. Nechaev[1] and E. E. Krasovskii[1,2,3]

[1]*Donostia International Physics Center (DIPC), Paseo Manuel de Lardizabal 4, 20018 Donostia/San Sebastián, Basque Country, Spain*

[2]*Departamento de Física de Materiales, Facultad de Ciencias Químicas, Universidad del Pais Vasco/Euskal Herriko Unibertsitatea, Apartado 1072, 20080 Donostia/San Sebastián, Basque Country, Spain*

[3]*IKERBASQUE, Basque Foundation for Science, 48013 Bilbao, Basque Country, Spain*

(Received 17 June 2019; published 24 September 2019)

An effective $\mathbf{k}\cdot\mathbf{p}$ Hamiltonian is applied to spin-orbit-split states in the surface alloys $PbAg_2$ and $BiAg_2$ on Ag(111) with the aim to infer the microscopic mechanism behind the momentum dependence of the spin polarization beyond the standard Rashba model. The Hamiltonian is derived from the *ab initio* wave functions at $\bar{\Gamma}$ without introducing any adjustable parameters so as to accurately reproduce the spin of the surface-alloy states, in particular the sign reversal of the spin polarization within a nondegenerate band. We establish the origin of the sign reversal and describe the spin-orbit splitting around $\bar{\Gamma}$ as a combination of the linear and cubic Rashba effects. Furthermore, we predict the behavior of the $PbAg_2$ and $BiAg_2$ states under the influence of an in-plane and out-of-plane magnetization for a surface alloy in contact with a magnetic layer. Apart from the surface-alloy states, we identify a substrate-related surface state originating from the same branch of the complex band structure as the surface state on a clean Ag(111).

DOI: 10.1103/PhysRevB.100.115432

I. INTRODUCTION

Since early observation of the giant spin-orbit splitting of the surface states on $BiAg_2$/Ag(111) [1,2] and $PbAg_2$/Ag(111) [3], the surface alloys at noble-metal surfaces have been extensively studied as materials with tunable Rashba-type spin-orbit splitting. Constant attention to the surface alloys is due to their complex spin structure [4–6], which can be controlled, e.g., by molecular adsorption [7,8].

Following the seminal paper by LaShell *et al.* [9], the classical two-band Rashba Hamiltonian was used to qualitatively characterize two-dimensional (2D) spin-orbit-split states at the $PbAg_2$/Ag(111) and $BiAg_2$/Ag(111) surfaces, although with a reservation that the k-linear Rashba model is incapable of explaining the observed situation in all its complexity [2,10–15]. A distinctive feature here is that the in-plane spin projection changes sign within a branch of a spin-orbit split state. While some simple qualitative explanations have been suggested of the giant splitting of the surface states, including speculations about the role of in-plane and out-of-plane potential gradient, no attempt has been made to develop a transparent picture of the even more puzzling behavior of the in-plane spin.

An attempt to include higher-order contributions to the two-band Hamiltonian in describing the splitting of the states beyond the linear Rashba model (see, e.g., Ref. [16]) has made it possible to reproduce the hexagonal warping of the constant energy contours, but not the actual in-plane spin structure. In spite of the evident failure of the classical Rashba model to describe the spin-orbit effects in the surface alloys, they are still often considered as a Rashba system with strong spin-orbit interaction (SOI) described by two parameters: the Rashba energy E_R and the momentum offset k_R or, equivalently, by the Rashba parameter $\alpha_R = 2E_R/k_R$ and the effective mass $m^* = k_R/\alpha_R$.

The interest in the 2D states of the surface alloys remains high because they possess a rather small negative effective mass accompanied by a giant SOI-induced splitting with nontrivial spin structure. Current experimental technologies make it possible to grow the alloys on a substrate with a magnetic or nonmagnetic supporting layer for exploiting them as a functional 2D electronic element integrated in a complex layer structure. Thus, it is helpful to have a simple model that contains the essential physics underlying the spin-related properties of the surface alloys in order to propose technological combinations with other 2D materials and judge their performance. This calls for the development of an effective $\mathbf{k}\cdot\mathbf{p}$ model for the 2D states of $PbAg_2$ and $BiAg_2$, which facilitates the treatment of these alloys as part of a nanodevice, also in contact with a magnetic component.

In this paper, we apply our *ab initio* $\mathbf{k}\cdot\mathbf{p}$ perturbation approach [17,18] to the surface alloys $PbAg_2$ and $BiAg_2$ on the Ag(111) substrate in order to generate an effective Hamiltonian capable of providing accurate and comprehensive description of all spin-structure features of the surface-alloy states. We use the minimal basis set of *ab initio* spinor wave functions at $\bar{\Gamma}$—three pairs of spin-orbit-split states in the L-projected bulk band gap of the substrate. These states exist both in an alloy on a noble-metal surface [2,10,15] and in a stand-alone alloy layer [19,20]. In our *ab initio* calculations, we find that, in addition to the alloy-related states, on the $PbAg_2$/Ag(111) and $BiAg_2$/Ag(111) surfaces, there exists a substrate-related surface state in the L gap of Ag(111), which originates from the same branch of the complex band structure as the surface state on the clean Ag(111). It demonstrates a

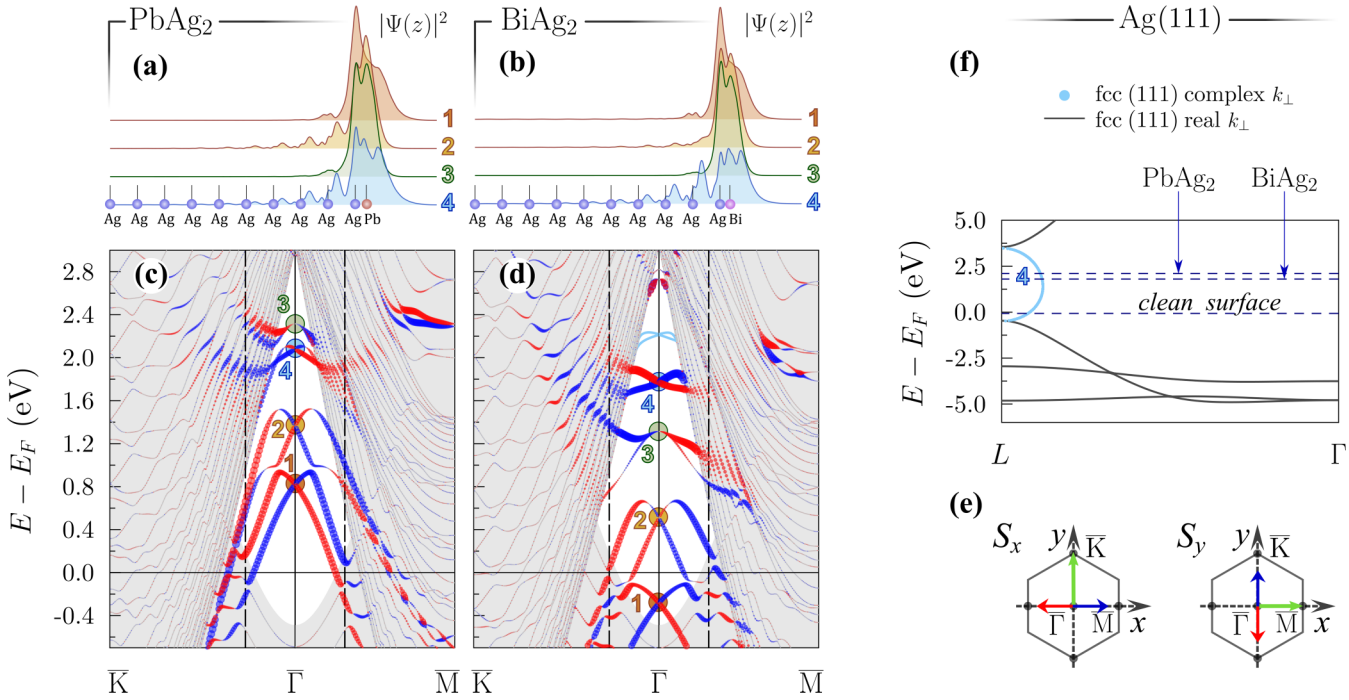

FIG. 1. Density profiles $|\Psi(z)|^2$ of the states of the surface alloys $PbAg_2$/Ag(111) (a) and $BiAg_2$/Ag(111) (b) at $\bar{\Gamma}$. Shown is the upper half of the symmetric 21-layer slab simulating the surface of the alloys. Band structure of $PbAg_2$/Ag(111) (c) and $BiAg_2$/Ag(111) (d) along $\bar{\Gamma}$-$\bar{K}$ and $\bar{\Gamma}$-$\bar{M}$ by the full *ab initio* Hamiltonian $H_{\mathbf{k}}^{\mathrm{LDA}}$ is presented by fat bands showing the spin polarization calculated as the expectation value of in-plane spin over the upper half of the slab. For $BiAg_2$/Ag(111), the dispersion relation of the state $n = 4$ for the experimental buckling $\Delta z = 0.65$ Å [21] of the surface-alloy layer is shown by light blue lines. The shaded area covers the surface-projected bulk states of silver. (e) Color coding for the spin projections S_x and S_y relative to the directions (green arrows) of the surface Brillouin zone. (f) Complex band structure of Ag(111) at $\bar{\Gamma}$. Solid lines show Bloch states with $\mathrm{Im}[k_\perp] = 0$ for $k_\perp$ along the L-Γ line of the bulk fcc Brillouin zone. Light blue points indicate $\mathrm{Im}[k_\perp]$ of the evanescent waves in the L gap. Dashed lines mark the energies of the state $n = 4$ in $PbAg_2$/Ag(111) and $BiAg_2$/Ag(111) and the energy of the surface state on the clean Ag(111) surface.

typical Rashba splitting with the Rashba parameter α_R orders of magnitude larger than on the clean surface.

By reducing the Hilbert space of our effective model to only two pairs of the states at $\bar{\Gamma}$, we reveal that it is the $\mathbf{k}$-dependent hybridization with the $m_j = \pm\frac{3}{2}$ state that brings about the nontrivial spin structure. In order to obtain an explicit functional dependence of the splitting on $\mathbf{k}$ around $\bar{\Gamma}$, we further reduce the basis to one pair but, at the same time, include third-order in k terms of the relativistic $\mathbf{k}\cdot\mathbf{p}$ expansion derived from microscopic spinor wave functions. Finally, we study the behavior of a surface alloy brought into contact with a magnetic material, namely how the 2D states are influenced by an in-plane and out-of-plane magnetization of supporting magnetic layers. We show that the effect of the out-of-plane magnetization on the spin z projection is very different from the case of a classical Rashba-split state.

II. METHOD AND RESULTS

We consider two surface alloys $PbAg_2$ and $BiAg_2$ of the $(\sqrt{3}\times\sqrt{3})R30^\circ$ structure at the Ag(111) surface. We simulate each surface alloy by a centrosymmetric 21-layer slab of space group $P\bar{3}1m$ (no. 162). The slab consists of a 17-layer Ag(111) substrate and the surface alloy composed of two atomic layers, Ag and Pb (Bi), at both sides of the substrate. We use the experimental crystal lattice parameter of silver with the buckling of the surface-alloy layers ($\Delta z = 0.97$ Å for $PbAg_2$ and 0.85 Å for $BiAg_2$) taken from Ref. [10]. Band-structure calculations are performed with the extended linear augmented plane-wave method [22] (the accuracy of the wave functions is essential for the efficiency of our $\mathbf{k}\cdot\mathbf{p}$ methods) within the local density approximation (LDA) for the exchange-correlation functional using the full potential scheme of Ref. [23].

Figure 1 shows the calculated spin-resolved band structure of the surface alloys along $\bar{\Gamma}$-$\bar{K}$ and $\bar{\Gamma}$-$\bar{M}$. Historically [10,12], in the L-projected bulk band gap [the folded L gap of the Ag(111) substrate] of the $PbAg_2$/Ag(111) and $BiAg_2$/Ag(111) band structure four spin-orbit split surface states are identified. Three of them have the dominant contribution from Pb (Bi) atoms and are classified as sp_z, $m_j = \frac{1}{2}$, and $m_j = \frac{3}{2}$ according to their orbital character. These are the states the majority of the theoretical and experimental studies of the surface alloys have been focused on. Below, we refer to these states as the surface-alloy states because of their almost complete localization in the $PbAg_2$ ($BiAg_2$) layer, Figs. 1(a) and 1(b), and because they are present in the spectrum of the surface alloys both with and without the Ag(111) substrate [19,20]. In Fig. 1 and hereinafter, the surface-alloy states that appear at $\bar{\Gamma}$ as three degenerate Kramers pairs $|\Phi_{n\mu}\rangle$ with $n = 1$, 2, and 3 are numbered in order of increasing energy at $\bar{\Gamma}$. The subscript μ, which refers to a member

of a pair, will be omitted for brevity when a discrimination between the members of the pair is not required. We use this numbering instead of the angular-momentum notation with the following correspondence: $sp_z \to 1$, $m_j = \frac{1}{2} \to 2$, and $m_j = \frac{3}{2} \to 3$ [24].

All the surface-alloy states are rather strongly localized in the Pb (Bi) atomic sphere. In this sphere, for the state $|\Phi_1\rangle$ the contribution of p orbitals is much larger than of s orbitals, and the weight of p_z orbitals is comparable to the total contribution of p_x and p_y ones. For $|\Phi_2\rangle$, the s contribution is still smaller, and the sum of p_x and p_y strongly dominates over p_z. The $|\Phi_3\rangle$ state is an atomiclike $m_j = \pm\frac{3}{2}$ state with the wave function of purely $p_{x,y}$ character. Note that the states $|\Phi_1\rangle$ and $|\Phi_2\rangle$ have appreciable contribution of s character in the Ag spheres of the surface-alloy layer.

The fourth state, $|\Phi_4\rangle$, lies well above the Fermi level, and in Ref. [10] it was described as a p_z-like surface state that penetrates deep into the bulk, in accord with our calculations, Figs. 1(a) and 1(b). We assign the number "4" to this state irrespective of its energy position relative to the surface-alloy states ($n = 1$, 2, and 3). In Ref. [6], this state was claimed to be observed with two-photon photoemission in $BiAg_2/Ag(111)$ at 2.6 eV above the Fermi energy (which is about 0.8 eV higher than in the calculations of Ref. [10]), while in Ref. [25] a state seen at this energy in inverse photoemission was identified as a Ag(111) surface-umklapp band. Our calculations show that $|\Phi_4\rangle$ derives from the complex band structure (CBS) of the Ag(111) substrate, see Fig. 1(f), although it has an appreciable weight in the alloy layers.

Apart from the usual calculation for a finite-thickness slab, we have applied the embedding method of Refs. [26,27], in which the semi-infinite Ag(111) substrate is represented by its complex band structure. This proves that the asymptotics of $|\Phi_4\rangle$ in the bulk is a single evanescent wave, which belongs to the same branch of the CBS as the well-studied surface state on the clean Ag(111) [28], while this branch does not contribute to the asymptotics of $|\Phi_1\rangle$, $|\Phi_2\rangle$, and $|\Phi_3\rangle$. It should be noted that this state is very sensitive to the geometry of the alloy layers. For the experimental $BiAg_2$ buckling $\Delta z = 0.65$ Å [21], the surface-state energy is 2.2 eV [light blue lines in the spectrum of $BiAg_2/Ag(111)$ in Fig. 1(d)], which is much closer to the experimental energy of Refs. [25] and [6]. At the same time, the energies of the surface-alloy states change only slightly. Thus, similar to noble-metal/organic interfaces [29–33], the "Shockley-type" surface state of the clean Ag(111) surface shifts to higher energies in the presence of the surface alloy.

Now, we turn to the spin structure of the surface-alloy states; see Figs. 1(c) and 1(d). Here, a special focus is usually put on the fact that the spin polarization changes sign at one point in a nondegenerate branch of a spin-orbit split state, whereby over a rather large momentum-energy range both spin-orbit split branches have the same sign of the spin projection perpendicular to $\mathbf{k}$ [5,10,12,14]. Following Ref. [10], two types of splitting of the surface-alloy states at $\bar{\Gamma}$ can be distinguished: a k-linear or classical Rashba splitting (for the states $n = 1$ and 2) and a nonlinear (k-cubic) splitting (for the state $n = 3$) characteristic of two-dimensional heavy-hole

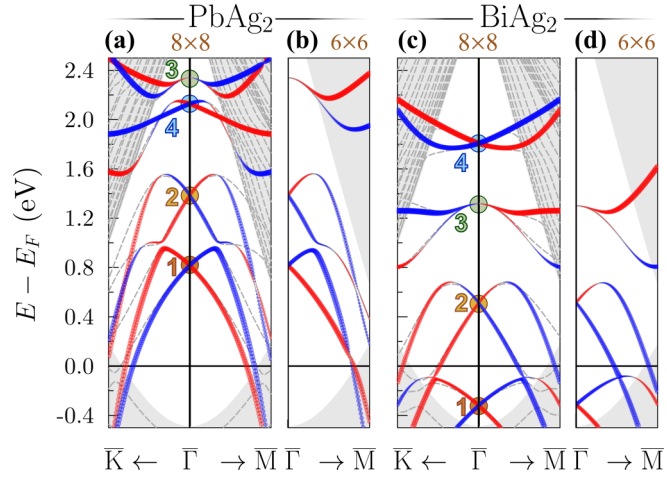

FIG. 2. Band structure of the surface alloys $PbAg_2$, (a) and (b), and $BiAg_2$, (c) and (d). Graphs (a) and (c) show eigenvalues of the eight-band and (b) and (d) of the six-band $\mathbf{k}\cdot\mathbf{p}$ Hamiltonians. In graphs (a) and (c), the surface-alloy band structures by the full *ab initio* Hamiltonian $H_{\mathbf{k}}^{\mathrm{LDA}}$ are presented by gray dashed lines. Thick lines show the spin projection S_y for $\mathbf{k}$ along $\bar{\Gamma}$-$\bar{M}$ and S_x for $\mathbf{k}$ along $\bar{\Gamma}$-$\bar{K}$. Positive values are given in red and negative in blue. The limits of the momentum intervals are indicated by vertical dashed lines in Figs. 1(c) and 1(d). Color code for spin is shown in Fig. 1(e).

systems [34–37]. Obviously, the traditional two-band Rashba Hamiltonian is not sufficient here, so we will employ an *ab initio* approach [17,18] to construct an effective $\mathbf{k}\cdot\mathbf{p}$ model around $\bar{\Gamma}$ and show that it describes both types of splitting and is capable of accurately reproducing the curious features of the spin polarization of the surface-alloy states.

First, for the reduced Hilbert space of the effective model we choose the basis that comprises all the four states at $\bar{\Gamma}$, i.e., eight *ab initio* spinor wave functions $|\Phi_{n\mu}\rangle$ with $n = 1$, 2, 3, and 4 and $\mu = \uparrow$ or $\downarrow$, the latter now indicating the z projection of the expectation value of the total angular momentum of a member of a pair (for details please see Refs. [17,18]). In Figs. 2(a) and 2(c), we show the spin-resolved band structure of $PbAg_2/Ag(111)$ and $BiAg_2/Ag(111)$, respectively, obtained by diagonalizing this Hamiltonian. As seen in the figures, the eight-band model has absorbed all the microscopic information, so it closely reproduces both the spin-orbit splitting of the states around $\bar{\Gamma}$ and their *true* spin structure. Then we further minimize the size of the $\mathbf{k}\cdot\mathbf{p}$ Hamiltonian by excluding the silver surface state $|\Phi_4\rangle$ because it is related to the substrate and examine whether a six-band model can reproduce the dispersion and spin polarization of the surface-alloy states ($n = 1$, 2, and 3). Here, we just note that the Rashba parameter of $|\Phi_4\rangle$ is 1.05 eV Å in Pb/Ag(111) and 0.96 eV Å in Bi/Ag(111), which is about 30 times larger than 0.031 eV Å, experimentally determined for a clean Ag(111) surface [38].

We now focus on the six-dimensional subspace $|\Phi_{n\mu}\rangle$, $n = 1$, 2, and 3, spanned by the surface-alloy states. The microscopically derived $\mathbf{k}\cdot\mathbf{p}$ Hamiltonian has the form

$$H_{\mathbf{kp}} = \left(\begin{array}{cc|c} E_1 + H_1 & H_0 + H_V & \widetilde{H}_1 \\ H_0^\dagger + H_V^\dagger & E_2 + H_2 & \widetilde{H}_2 \\ \hline \widetilde{H}_1^\dagger & \widetilde{H}_2^\dagger & E_3 + H_3 \end{array}\right), \qquad (1)$$

where $E_n = \epsilon_n \mathbb{I}_{2\times 2}$ and

$$H_n = \begin{pmatrix} M_n k^2 & i\alpha_n k_- \\ -i\alpha_n k_+ & M_n k^2 \end{pmatrix}, \quad H_V = \begin{pmatrix} 0 & iVk_+^2 \\ iVk_-^2 & 0 \end{pmatrix}$$

with $k_\pm = k_x \pm ik_y$ and $k = \sqrt{k_x^2 + k_y^2}$. The coupling between the states $n = 1,\ 2$ and the state $n = 3$ is described by the term

$$\widetilde{H}_n = \begin{pmatrix} -i\tilde{\alpha}_n k_+ - iN_n k_-^2 & \delta_n k_+ + D_n k_-^2 \\ \delta_n k_- - D_n k_+^2 & -i\tilde{\alpha}_n k_- + iN_n k_+^2 \end{pmatrix}.$$

The related spin matrix that yields the *true* spin structure has the form

$$\mathbf{S_{kp}} = \left(\begin{array}{cc|c} \mathbf{S}_1 & \mathbf{S}_0 & \widetilde{\mathbf{S}}_1 \\ \mathbf{S}_0 & \mathbf{S}_2 & \widetilde{\mathbf{S}}_2 \\ \hline \widetilde{\mathbf{S}}_1^* & \widetilde{\mathbf{S}}_2^* & \mathbf{S}_3 \end{array}\right) \tag{2}$$

with $\mathbf{S}_n = (s_n^\parallel \boldsymbol{\sigma}_\parallel, s_n^z \sigma_z)$, $\widetilde{\mathbf{S}}_n = \tilde{s}_n^\parallel \exp(i\pi\sigma_y/2)\boldsymbol{\sigma}_\parallel$, and $\boldsymbol{\sigma}_\parallel = (\sigma_x, \sigma_y)$, where σ_x, σ_y, and σ_z are the Pauli matrices. The elements of the spin matrix enter into the definition of the spin expectation value

$$\langle \mathbf{S}_{\mathbf{k}\lambda} \rangle = \frac{1}{2} \sum_{n\mu l\nu} C^{\lambda *}_{\mathbf{k}n\mu} C^{\lambda}_{\mathbf{k}l\nu} [\mathbf{S_{kp}}]^{n\mu}_{l\nu} \tag{3}$$

in the state $|\widetilde{\Phi}^\lambda_{\mathbf{k}}\rangle = \sum_{n\mu} C^\lambda_{\mathbf{k}n\mu} |\Phi_{n\mu}\rangle$ of the reduced Hilbert space of the Hamiltonian (1). The six-dimensional vectors $\mathbf{C}^\lambda_{\mathbf{k}}$ diagonalize the Hamiltonian, $H_{\mathbf{kp}}\mathbf{C}^\lambda_{\mathbf{k}} = E^\lambda_{\mathbf{k}}\mathbf{C}^\lambda_{\mathbf{k}}$. For the surface alloys, the parameters in Eq. (1) are listed in Table I. The band structure $E^\lambda_{\mathbf{k}}$ obtained with these parameters is presented in Figs. 2(b) and 2(d) by fat bands showing the spin polarization of the spin-orbit split surface-alloy states obtained from Eq. (3). As seen in the figure, the microscopically derived six-band $\mathbf{k}\cdot\mathbf{p}$ model nicely reproduces all the specific features of the observable spin structure of the states under study, although far from $\bar{\Gamma}$ the dispersion is distorted.

TABLE I. Parameters of the six- and two-band $\mathbf{k}\cdot\mathbf{p}$ Hamiltonian (based on calculations for centrosymmetric 21-layer slabs with the lattice parameter $a = 9.466$ a.u. for $PbAg_2$ and $BiAg_2$). We use Rydberg atomic units: $\hbar = 2m_0 = e^2/2 = 1$.

	$PbAg_2$	$BiAg_2$
ϵ_1	0.060	−0.024
ϵ_2	0.101	0.037
ϵ_3	0.169	0.095
α_1	−0.392	−0.357
α_2	0.566	0.507
α_3	0.000	0.000
$\tilde{\alpha}_1$	−0.415	−0.356
$\tilde{\alpha}_2$	0.454	0.385
δ_1	0.015	0.011
δ_2	0.014	0.008
α_0	−0.027	−0.035
M_1	−0.98	−0.33
M_2	−1.39	−0.91
M_3	−12.16	−7.99
D_1/N_1	1.16/−0.20	−0.96/−0.05
D_2/N_2	−0.29/0.27	−0.10/0.10
M_0/V	−1.74/0.19	−2.36/0.10
$\alpha_1^{(3)}$	1.57	1.27
$\alpha_2^{(3)}$	−37.43	−32.70
$\alpha_3^{(3)}$	0.00	0.00
$\mathcal{M}_1$	−2.47	−1.35
$\mathcal{M}_2$	−4.16	−3.29
$\mathcal{M}_3$	−7.48	−4.34
W_1	−0.14	−0.07
W_2	0.81	0.57
W_3	3.52	0.19
η/θ	−30.02/8.87	−18.93/-2.10
$s_1^\parallel/s_1^z$	0.72/0.44	0.64/0.28
$s_2^\parallel/s_2^z$	0.58/0.16	0.49/−0.03
$s_3^\parallel/s_3^z$	0.00/1.00	0.00/1.00
$\tilde{s}_1^\parallel/\tilde{s}_2^\parallel$	0.51/0.64	0.58/0.71
$s_0^\parallel/s_0^z$	−0.34/−0.68	−0.42/−0.85

III. DISCUSSION AND CONCLUSIONS

Owing to the possibility to choose physically relevant states to span the model Hilbert space, the *ab initio* approach elucidates the role of the hybridization between the basis states in the formation of the spin polarization and reveals the importance of each individual state for spin texture. In Figs. 3(a) and 3(d), we show the eigenvalues $E^\lambda_{\mathbf{k}}$ of the six-band Hamiltonian (1) with the contributions $\sum_\mu |C^\lambda_{\mathbf{k}n\mu}|^2$ of each basis state presented by brown, orange, and green fat bands for $n = 1$, 2, and 3, respectively. The figures show that over an interval around $\bar{\Gamma}$ in both surface alloys there is a tangible hybridization of the state $n = 3$ with other two states ($3 \leftrightarrow 1$ and $3 \leftrightarrow 2$), while the states $n = 1$ and 2 considerably hybridize ($1 \leftrightarrow 2$) only in $PbAg_2$. Thus, since the in-plane spin changes sign in both alloys, the $2 \leftrightarrow 1$ hybridization can hardly be considered responsible for the sign reversal.

To get insight into the role of the hybridization in the spin polarization, we reduce the dimension of the effective model to a four-band Hamiltonian. In Figs. 3(b) and 3(e), we plot the spin-resolved bands of the selected surface-alloy states. As seen in the figures, the $3 \leftrightarrow 1$ or $3 \leftrightarrow 2$ hybridization leads to the changes in the spin polarization in the outer branch of the spin-orbit split states $n = 1$ and 2. In turn, as a result of the hybridization both branches of the state $n = 3$ adopt the polarization of the outer branch of the state, with which it hybridizes. Therefore, the resulting spin polarization of the state $n = 3$, Fig. 2, varies with the momentum $\mathbf{k}$ in accordance with the weights of the lower-lying surface-alloy states shown in Figs. 3(a) and 3(d).

The four-band Hamiltonian for the lowest bands allows us to examine the $2 \leftrightarrow 1$ hybridization, which was experimentally studied in Ref. [15]. The respective panels in Figs. 3(b) and 3(e) show the avoided crossing (more pronounced in $PbAg_2$) due to the same spin of the outer branch of the state $n = 1$ and the inner branch of state $n = 2$ [both are blue in the $2 \leftrightarrow 1$ panels in Figs. 3(b) and 3(e)]. This corresponds to the opposite sign of the Rashba parameters α_1 and α_2; see Table I. At the same time, no sign change is observed in the outer branches of the states involved in the four-band Hamiltonian. Thus, we can conclude that it is the hybridization of the state $n = 1$ and 2 with the state $n = 3$ that is responsible for

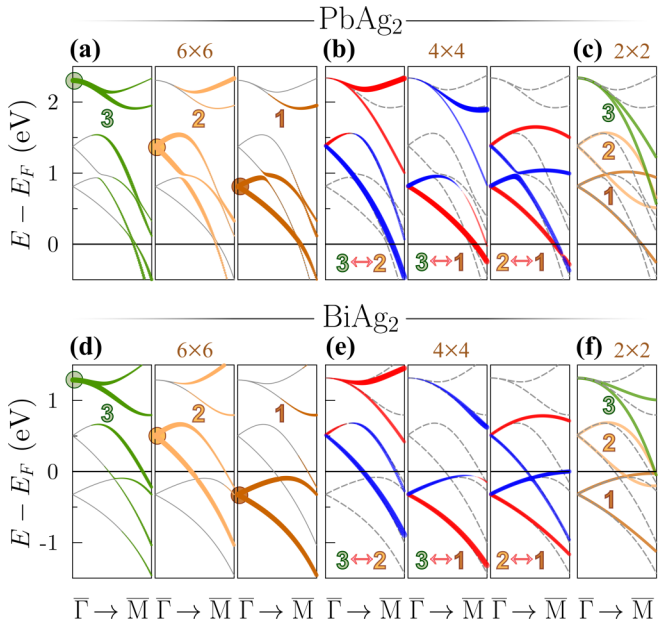

FIG. 3. Band structure of $PbAg_2$, upper row, and of $BiAg_2$, lower row, by small-size Hamiltonians. (a),(d) Eigenvalues of the six-band Hamiltonian (1). Brown, orange, and green fat bands highlight the contributions from the basis states $|\Phi_{n\uparrow(\downarrow)}\rangle$ with $n = 1$, 2, and 3, respectively. (b),(e) Fat bands show the positive (blue) and negative (red) values of S_y for three four-band Hamiltonians: $3 \leftrightarrow 2$, $3 \leftrightarrow 1$, and $2 \leftrightarrow 1$. (c),(f) Eigenvalues $E^{n\pm}_{\mathbf{k}}$ of the two-band Hamiltonian (see text). In graphs (b), (c), (e), and (f) the bands by the six-band $\mathbf{k}\cdot\mathbf{p}$ model are shown by dashed gray lines.

the observed spin structure, in sharp contrast to the classical Rashba effect.

We now take a closer look at the surface-alloy states around the $\bar{\Gamma}$ point, and further reduce the model Hilbert space to get two-band Hamiltonians. So far, we have used our *ab initio* approach based on the second-order $\mathbf{k}\cdot\mathbf{p}$ expansion around the reference point [17,18] in applying the Löwdin partitioning [39–41] to the original Hilbert space of the reference-point-projected LDA Hamiltonian $H^{\mathrm{LDA}}_{\mathbf{k}}$. Now, we further develop our approach by implementing a third-order $\mathbf{k}\cdot\mathbf{p}$ expansion to microscopically generate two-band Hamiltonians including terms to third order in k, thereby allowing for both linear and cubic Rashba effects in a two-band $\mathbf{k}\cdot\mathbf{p}$ model.

For the states $n = 1$ and 2, the two-band Hamiltonian has the following form:

$$H^{(3)}_n = \begin{pmatrix} \tilde{\epsilon}_n + W_n(k_+^3 + k_-^3) & i\gamma_n k_- \\ -i\gamma_n k_+ & \tilde{\epsilon}_n - W_n(k_+^3 + k_-^3) \end{pmatrix} \quad (4)$$

with $\tilde{\epsilon}_n = \epsilon_n + \mathcal{M}_n k^2$, the so-called "renormalized Rashba parameter" $\gamma_n = \alpha_n + \alpha_n^{(3)} k^2$, and "hexagonal warping term" characterized by the parameter W_n (the parameters are listed in Table I). Since the respective 2×2 spin matrix is $\mathbf{S}_n = (s^{\parallel}_n \boldsymbol{\sigma}_{\parallel}, s^z_n \sigma_z)$, one is tempted to rewrite the Hamiltonian $H^{(3)}_n$ with the use of the Pauli matrices and to associate these matrices with the observable spin, as

$$H^{(3)}_n = \tilde{\epsilon}_n \sigma_0 + \gamma_n(k_y\sigma_x - k_x\sigma_y) + W_n(k_+^3 + k_-^3)\sigma_z. \quad (5)$$

Here, one should take into account that the in-plane and out-of-plane spin polarization is within the limits of $\pm\frac{1}{2}s^{\parallel}_n$ and $\pm\frac{1}{2}s^z_n$, respectively (see Table I), so the Hamiltonian (5) is valid in the energy-momentum region around $\bar{\Gamma}$, where the *ab initio* spin polarization does not change sign. It is noteworthy that the Hamiltonian $H^{(3)}_n$ is in accord with the form of both the Hamiltonian constructed in Ref. [42] from the theory of invariants for surface states of the topological insulator Bi_2Te_3 [43] and the Hamiltonian suggested in Ref. [16] for the occupied surface-alloy state ($n = 1$ in our notation) of $BiAg_2/Ag(111)$. The eigenvalues of $H^{(3)}_n$ [brown and orange lines in Figs. 3(c) and 3(f)] can be written as

$$E^{n\pm}_{\mathbf{k}} = \tilde{\epsilon}_n \pm k\sqrt{\gamma_n^2 + 4W_n^2 k^4 \cos^2 3\varphi_{\mathbf{k}}},$$

where $\varphi_{\mathbf{k}}$ is the polar angle of the momentum $\mathbf{k}$. The SOI-induced splitting of the states $n = 1$ and 2 around $\bar{\Gamma}$ is, thereby, determined by the leading isotropic k-linear term with an anisotropic contribution governed by W_n.

The two-band Hamiltonian for the state $n = 3$ consists of the Hamiltonian $H^{(3)}_3$ of Eq. (4) with $\gamma_3 = 0$ and the additional term (similar to the cubic Rashba term [35,36,44])

$$H'_3 = \begin{pmatrix} 0 & i\theta(k_+^3 + k_-^3) + i\eta k_-^3 \\ -i\theta(k_+^3 + k_-^3) - i\eta k_+^3 & 0 \end{pmatrix}.$$

The 2×2 spin matrix is $\mathbf{S}_3 = (0, 0, \sigma_z)$ with zero in-plane matrix elements. This ensures the S_z spin polarization in accordance with the symmetry of the system. As follows from the expression for the eigenvalues

$$E^{3\pm}_{\mathbf{k}} = \tilde{\epsilon}_3 \pm k^3\sqrt{\eta^2 + 4\left(W_3^2 + \theta^2 + \eta\theta\right)\cos^2 3\varphi_{\mathbf{k}}},$$

shown in Figs. 3(c) and 3(f) by green lines, the splitting of the state $n = 3$ near the $\bar{\Gamma}$ point is purely cubic in k, and it depends on both the isotropic and anisotropic contributions (see the parameters in Table I). The in-plane spin projection for this state becomes finite due to the hybridization with other surface-alloy states only, which is not the case in our two-band consideration. Additionally, we would like to mention that the presented form of the two-band Hamiltonians can be easily obtained analytically by applying the Löwdin partitioning to the six- or four-band Hamiltonians we derived above. Note that our third-order $\mathbf{k}\cdot\mathbf{p}$ theory builds on the original *ab initio* Hamiltonian, with the basis being its eigenstates. Thus, the $\mathbf{k}\cdot\mathbf{p}$ expansion uniquely follows from the basis set: in particular, in contrast to a fitting method the shape of the third-order term does not depend on whether or not we include the fourth-order term (and does not affect the lower-order terms). This renders the third-order expansion physically meaningful, which is promising in view of the increasing interest in the cubic Rashba effect in semiconductor quantum wells [45,46] and at the oxide surfaces and interfaces [47–50].

Finally, we consider the effect of an external magnetic exchange field on the dispersion relation and spin polarization of the surface-alloy states. As in Refs. [51–53], the exchange field can be realized, e.g., by growing the surface alloy on a magnetic metal [54]. Similar to Refs. [18,55], we simulate the magnetic exchange interaction of strength J_{ex} with the magnetization $\mathbf{M}$ by the term $H^{\mathrm{EX}} = -J_{\mathrm{ex}}\mathbf{M}\cdot\mathbf{S}_{\mathbf{kp}}$ and treat $\mathcal{J} = J_{\mathrm{ex}}\mathbf{M}$ as a tunable parameter. In Fig. 4, we show the spectrum of the states under study for two orientations of the magnetization $\mathbf{M}$: the in-plane, $\mathbf{M}\downarrow\uparrow\hat{\mathbf{y}}$, and out-of-plane,

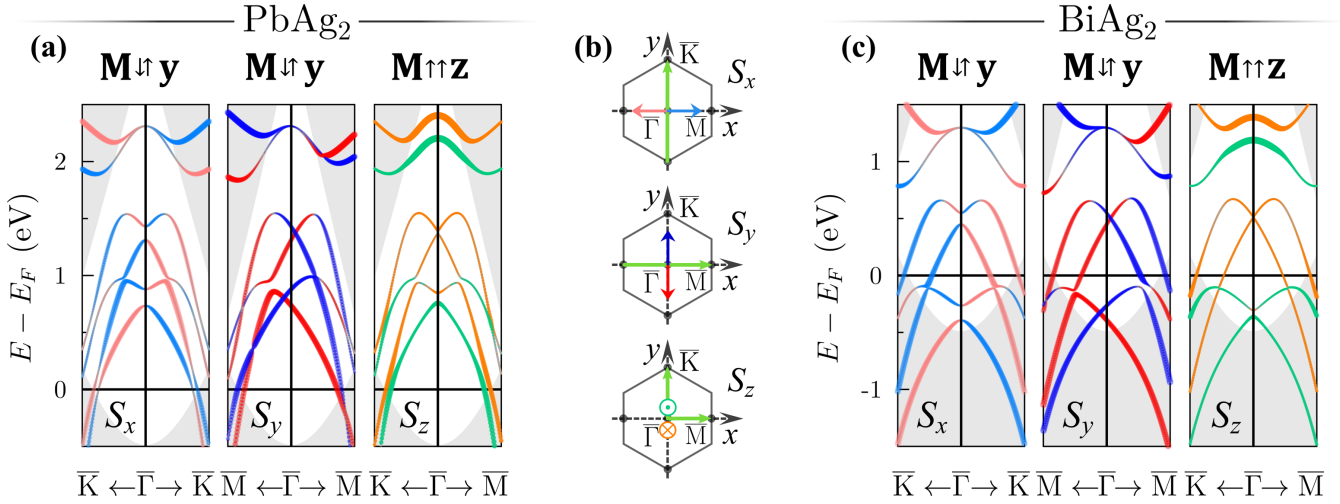

FIG. 4. Effect of external exchange (magnetic) interaction on the surface-alloy states of $PbAg_2$ (a) and $BiAg_2$ (c) for the in-plane, $\mathbf{M} \downarrow\uparrow \hat{\mathbf{y}}$, and out-of-plane, $\mathbf{M} \uparrow\uparrow \hat{\mathbf{z}}$, orientation of the magnetization $\mathbf{M}$. (b) Color code for spin polarization with reference to the momentum direction.

$\mathbf{M} \uparrow\uparrow \hat{\mathbf{z}}$, orientation. To make the effect more pronounced, we chose a rather large value of the exchange parameter, $\mathcal{J} = |\mathcal{J}| = 100$ meV.

As seen in the S_x and S_y panels in Figs. 4(a) and 4(c), similar to the Rashba-split surface states on magnetic metal surfaces [52,56], the in-plane magnetization causes a tangible asymmetry in the dispersion curves with respect to the $\bar{\Gamma}$ point for $\mathbf{k}$ perpendicular to the magnetization (along k_x, $\bar{M}$-$\bar{\Gamma}$-$\bar{M}$), and for the surface-alloy states $n = 1$ and 2 (which have finite $s_n^{\parallel}$ and α_n) it shifts the degeneracy points away from $\bar{\Gamma}$. For all states, at $\bar{\Gamma}$ there appear gaps of different width: rather pronounced gaps for the states $n = 1$ and 2 and a negligible gap for the state $n = 3$ caused by the nonzero coupling parameters $\tilde{s}_n^{\parallel}$. The in-plane spin polarization changes because the exchange term favors the collinear alignment of the spins with the magnetization and, thereby, creates an imbalance in the spins "up" and "down" along $\mathbf{M}$. However, the characteristic in-plane spin structure survives, implying that SOI dominates over the rather strong external exchange field.

The out-of-plane magnetization has a negligible effect on the symmetry of the spectrum owing to a small albeit finite S_z in the paramagnetic phase (not shown in Fig. 2) and for all surface-alloy states it eliminates a degeneracy point and creates a gap between the two branches; see the S_z panels in Figs. 4(a) and 4(c). Now, the state $n = 3$ has the largest gap, which for a given exchange parameter is determined solely by s_3^z. The gaps of the states $n = 1$, 2 are largely controlled by s_1^z and s_2^z, respectively, with an influence of the coupling parameter s_0^z. Therefore, the state $n = 2$ with its small s_2^z (see Table I) has a tiny splitting at $\bar{\Gamma}$. The in-plane spin polarization of the states remains unaffected, while the induced out-of-plane spin component exhibits an unexpected behavior [57]. Actually, while the two branches of the spin-orbit split state $n = 3$ have a large magnitude and opposite sign of the spin expectation value of the spin z projection S_z, both branches of each of the states $n = 1$, 2 have the same sign of S_z, which is relatively small in magnitude. As seen in the S_z panels in Figs. 4(a) and 4(c), apart from the small vicinity of $\bar{\Gamma}$ both branches of the state $n = 1$ have $S_z > 0$ and for $n = 2$ it is $S_z < 0$. Thus, the surface-alloy states are clearly distinguished by their response to the out-of-plane magnetization, while they mostly preserve their in-plane spin structure.

To summarize, we have developed an effective model for the 2D states of the surface alloys $PbAg_2$ and $BiAg_2$. The model is based on a fully *ab initio* $\mathbf{k} \cdot \mathbf{p}$ perturbation approach to generate model Hamiltonians of a desired size, and it provides accurate and comprehensive description of the spin structure of the states of interest. This approach has enabled us to reveal the origin of the puzzling behavior of the momentum-dependent spin polarization, namely the spin direction reversal within a branch of a spin-orbit split state. A novel aspect of the present approach is the *third order* in k perturbation expansion, which makes it possible to write down an explicit functional dependence of the splitting of the surface-alloy states on k around $\bar{\Gamma}$, accounting for both linear and cubic Rashba effects. Furthermore, we have demonstrated the capability of the effective models to predict the behavior of the surface-alloy states under the influence of in-plane and out-of-plane magnetization of possible supporting magnetic layers.

ACKNOWLEDGMENT

This work was supported by the Spanish Ministry of Science, Innovation and Universities (Project No. FIS2016-76617-P).

[1] C. R. Ast, D. Pacilé, M. Falub, L. Moreschini, M. Papagno, G. Wittich, P. Wahl, R. Vogelgesang, M. Grioni, and K. Kern, Giant Spin-Splitting in the Bi/Ag(111) Surface Alloy, arXiv:cond-mat/0509509 (2005).

[2] C. R. Ast, Jürgen Henk, A. Ernst, L. Moreschini, M. C. Falub, D. Pacilé, P. Bruno, K. Kern, and M. Grioni, Giant Spin Splitting through Surface Alloying, Phys. Rev. Lett. **98**, 186807 (2007).

[3] D. Pacilé, C. R. Ast, M. Papagno, C. Da Silva, L. Moreschini, M. Falub, A. P. Seitsonen, and M. Grioni, Electronic structure of an ordered Pb/Ag(111) surface alloy: Theory and experiment, Phys. Rev. B **73**, 245429 (2006).

[4] S. Schirone, E. E. Krasovskii, G. Bihlmayer, R. Piquerel, P. Gambardella, and A. Mugarza, Spin-Flip and Element-Sensitive Electron Scattering in the $BiAg_2$ Surface Alloy, Phys. Rev. Lett. **114**, 166801 (2015).

[5] R. Noguchi, K. Kuroda, K. Yaji, K. Kobayashi, M. Sakano, A. Harasawa, T. Kondo, F. Komori, and S. Shin, Direct mapping of spin and orbital entangled wave functions under interband spin-orbit coupling of giant Rashba spin-split surface states, Phys. Rev. B **95**, 041111(R) (2017).

[6] P. Rosenzweig, S. Otto, and T. Fauster, Complex manifold of Rashba and image-potential states on Bi/Ag(111), Phys. Rev. B **98**, 085430 (2018).

[7] R. Friedrich, V. Caciuc, B. Zimmermann, G. Bihlmayer, N. Atodiresei, and S. Blügel, Creating anisotropic spin-split surface states in momentum space by molecular adsorption, Phys. Rev. B **96**, 085403 (2017).

[8] R. Friedrich, V. Caciuc, G. Bihlmayer, N. Atodiresei, and S. Blügel, Designing the Rashba spin texture by adsorption of inorganic molecules, New J. Phys. **19**, 043017 (2017).

[9] S. LaShell, B. A. McDougall, and E. Jensen, Spin Splitting of an Au(111) Surface State Band Observed with Angle Resolved Photoelectron Spectroscopy, Phys. Rev. Lett. **77**, 3419 (1996).

[10] G. Bihlmayer, S. Blügel, and E. V. Chulkov, Enhanced Rashba spin-orbit splitting in Bi/Ag(111) and Pb/Ag(111) surface alloys from first principles, Phys. Rev. B **75**, 195414 (2007).

[11] C. R. Ast, D. Pacilé, L. Moreschini, M. C. Falub, M. Papagno, K. Kern, M. Grioni, J. Henk, A. Ernst, S. Ostanin, and P. Bruno, Spin-orbit split two-dimensional electron gas with tunable Rashba and Fermi energy, Phys. Rev. B **77**, 081407(R) (2008).

[12] H. Bentmann, F. Forster, G. Bihlmayer, E. V. Chulkov, L. Moreschini, M. Grioni, and F. Reinert, Origin and manipulation of the Rashba splitting in surface alloys, Europhys. Lett. **87**, 37003 (2009).

[13] F. Meier, V. Petrov, S. Guerrero, C. Mudry, L. Patthey, Jürg Osterwalder, and J. H. Dil, Unconventional Fermi surface spin textures in the Bi_xPb_{1-x}/Ag(111) surface alloy, Phys. Rev. B **79**, 241408(R) (2009).

[14] H. Mirhosseini, J. Henk, A. Ernst, S. Ostanin, C.-T. Chiang, P. Yu, A. Winkelmann, and J. Kirschner, Unconventional spin topology in surface alloys with Rashba-type spin splitting, Phys. Rev. B **79**, 245428 (2009).

[15] H. Bentmann, S. Abdelouahed, M. Mulazzi, J. Henk, and F. Reinert, Direct Observation of Interband Spin-Orbit Coupling in a Two-Dimensional Electron System, Phys. Rev. Lett. **108**, 196801 (2012).

[16] Sz. Vajna, E. Simon, A. Szilva, K. Palotas, B. Ujfalussy, and L. Szunyogh, Higher-order contributions to the Rashba-Bychkov effect with application to the Bi/Ag(111) surface alloy, Phys. Rev. B **85**, 075404 (2012).

[17] I. A. Nechaev and E. E. Krasovskii, Relativistic k · p Hamiltonians for centrosymmetric topological insulators from *ab initio* wave functions, Phys. Rev. B **94**, 201410(R) (2016).

[18] I. A. Nechaev and E. E. Krasovskii, Relativistic splitting of surface states at Si-terminated surfaces of the layered intermetallic compounds RT_2Si_2 (R=rare earth; T=Ir, Rh), Phys. Rev. B **98**, 245415 (2018).

[19] G. Bian, X. Wang, T. Miller, and T.-C. Chiang, Origin of giant Rashba spin splitting in Bi/Ag surface alloys, Phys. Rev. B **88**, 085427 (2013).

[20] N. Yamaguchi, H. Kotaka, and F. Ishii, First-principles study of Rashba effect in ultra-thin bismuth surface alloys, in *The 18th International Conference on Crystal Growth and Epitaxy (ICCGE-18)* [J. Cryst. Growth **468**, 688 (2017)].

[21] I. Gierz, B. Stadtmüller, J. Vuorinen, M. Lindroos, F. Meier, J. H. Dil, K. Kern, and C. R. Ast, Structural influence on the Rashba-type spin splitting in surface alloys, Phys. Rev. B **81**, 245430 (2010).

[22] E. E. Krasovskii, Accuracy and convergence properties of the extended linear augmented-plane-wave method, Phys. Rev. B **56**, 12866 (1997).

[23] E. E. Krasovskii, F. Starrost, and W. Schattke, Augmented fourier components method for constructing the crystal potential in self-consistent band-structure calculations, Phys. Rev. B **59**, 10504 (1999).

[24] While we focus here on the behavior of a Bloch electron near the nuclei, we keep in mind that the crystal breaks the rotation symmetry of a free atom, so we refrain from using the atomic-orbital terminology $|jm_j\rangle$ to refer to the Bloch states.

[25] S. N. P. Wissing, A. B. Schmidt, H. Mirhosseini, J. Henk, C. R. Ast, and M. Donath, Ambiguity of Experimental Spin Information from States with Mixed Orbital Symmetries, Phys. Rev. Lett. **113**, 116402 (2014).

[26] E. E. Krasovskii and W. Schattke, Angle-Resolved Photoemission from Surface States, Phys. Rev. Lett. **93**, 027601 (2004).

[27] E. E. Krasovskii, Augmented-plane-wave approach to scattering of Bloch electrons by an interface, Phys. Rev. B **70**, 245322 (2004).

[28] J. Lobo-Checa, J. E. Ortega, A. Mascaraque, E. G. Michel, and E. E. Krasovskii, Effect of photoelectron mean free path on the photoemission cross-section of Cu(111) and Ag(111) Shockley states, Phys. Rev. B **84**, 245419 (2011).

[29] C. H. Schwalb, S. Sachs, M. Marks, A. Schöll, F. Reinert, E. Umbach, and U. Höfer, Electron Lifetime in a Shockley-Type Metal-Organic Interface State, Phys. Rev. Lett. **101**, 146801 (2008).

[30] N. L. Zaitsev, I. A. Nechaev, and E. V. Chulkov, Change in surface states of Ag(111) thin films upon adsorption of a monolayer of PTCDA organic molecules, J. Exp. Theor. Phys. **110**, 114 (2010).

[31] M. Marks, N. L. Zaitsev, B. Schmidt, C. H. Schwalb, A. Schöll, I. A. Nechaev, P. M. Echenique, E. V. Chulkov, and U. Höfer, Energy shift and wave function overlap of metal-organic interface states, Phys. Rev. B **84**, 081301(R) (2011).

[32] N. L. Zaitsev, I. A. Nechaev, P. M. Echenique, and E. V. Chulkov, Transformation of the Ag(111) surface state due to molecule-surface interaction with ordered organic molecular monolayers, Phys. Rev. B **85**, 115301 (2012).

[33] S. S. Tsirkin, N. L. Zaitsev, I. A. Nechaev, R. Tonner, U. Höfer, and E. V. Chulkov, Inelastic decay of electrons in Shockley-type metal-organic interface states, Phys. Rev. B **92**, 235434 (2015).

[34] R. Winkler, Rashba spin splitting in two-dimensional electron and hole systems, Phys. Rev. B **62**, 4245 (2000).

[35] R. Winkler, H. Noh, E. Tutuc, and M. Shayegan, Anomalous Rashba spin splitting in two-dimensional hole systems, Phys. Rev. B **65**, 155303 (2002).

[36] J. Schliemann and D. Loss, Spin-Hall transport of heavy holes in III-V semiconductor quantum wells, Phys. Rev. B **71**, 085308 (2005).

[37] J. Li, W. Yang, and K. Chang, Spin states in InAs/AlSb/GaSb semiconductor quantum wells, Phys. Rev. B **80**, 035303 (2009).

[38] K. Yaji, A. Harasawa, K. Kuroda, R. Li, B. Yan, F. Komori, and S. Shin, Rashba spin splitting of L-gap surface states on Ag(111) and Cu(111), Phys. Rev. B **98**, 041404(R) (2018).

[39] P.-O. Löwdin, A Note on the Quantum-Mechanical Perturbation Theory, J. Chem. Phys. **19**, 1396 (1951).

[40] J. R. Schrieffer and P. A. Wolff, Relation between the Anderson and Kondo Hamiltonians, Phys. Rev. **149**, 491 (1966).

[41] R. Winkler, *Spin-Orbit Coupling Effects in Two-Dimensional Electron and Hole Systems* (Springer, Berlin, 2003).

[42] L. Fu, Hexagonal Warping Effects in the Surface States of the Topological Insulator Bi_2Te_3, Phys. Rev. Lett. **103**, 266801 (2009).

[43] For surface states of three-dimensional topological insulators, within our third-order expansion we obtain the two-band Hamiltonian $H_{2\times2} = (C_0 + C_{||}k^2)\sigma_0 - (V_{||} + V_{||}^{(3)}k^2)(k_y\sigma_x - k_x\sigma_y) - iW(k_+^3 - k_-^3)\sigma_z$ with k_x directed along $\bar{\Gamma}$-$\bar{M}$. Apart from the parameters C_0, $C_{||}$, and $V_{||}$ reported in Ref. [17] and the spin matrices obtained in Ref. [18] (see Ref. [29] therein) for six-quintuple-layer slabs, the surface states of Bi_2Se_3, Bi_2Te_3, and Sb_2Te_3 are additionally characterized by the renormalized velocity parameter $V_{||}^{(3)} = 27.81$, 4.86, and 32.14 a.u. and the hexagonal warping parameter $W = 5.80$, 22.84, and 52.05 a.u., respectively.

[44] L. G. Gerchikov and A.V. Subashiev, Spin splitting of size-quantization subbands in asymmetric heterostructures, Sov. Phys. Semicond. **26**, 73 (1992).

[45] R. Moriya, K. Sawano, Y. Hoshi, S. Masubuchi, Y. Shiraki, A. Wild, C. Neumann, G. Abstreiter, D. Bougeard, T. Koga, and T. Machida, Cubic Rashba Spin-Orbit Interaction of a Two-Dimensional Hole Gas in a Strained-Ge/SiGe Quantum Well, Phys. Rev. Lett. **113**, 086601 (2014).

[46] H. Liu, E. Marcellina, A. R. Hamilton, and D. Culcer, Strong Spin-Orbit Contribution to the Hall Coefficient of Two-Dimensional Hole Systems, Phys. Rev. Lett. **121**, 087701 (2018).

[47] H. Nakamura, T. Koga, and T. Kimura, Experimental Evidence of Cubic Rashba Effect in an Inversion-Symmetric Oxide, Phys. Rev. Lett. **108**, 206601 (2012).

[48] J. Varignon, L. Vila, A. Barthélémy, and M. Bibes, A new spin for oxide interfaces, Nat. Phys. **14**, 322 (2018).

[49] S. Gariglio, A. D. Caviglia, J.-M. Triscone, and M. Gabay, A spin-orbit playground: Surfaces and interfaces of transition metal oxides, Rep. Prog. Phys. **82**, 012501 (2018).

[50] W. Lin, L. Li, F. Doğan, C. Li, Hélène Rotella, X. Yu, B. Zhang, Y. Li, W. Siang Lew, S. Wang, W. Prellier, S. J. Pennycook, J. Chen, Z. Zhong, A. Manchon, and T. Wu, Interface-based tuning of Rashba spin-orbit interaction in asymmetric oxide heterostructures with $3d$ electrons, Nat. Commun. **10**, 3052 (2019).

[51] J. C. Rojas Sánchez, L. Vila, G. Desfonds, S. Gambarelli, J. P. Attané, J. M. De Teresa, C. Magén, and A. Fert, Spin-to-charge conversion using Rashba coupling at the interface between non-magnetic materials, Nat. Commun. **4**, 2944 (2013).

[52] C. Carbone, P. Moras, P. M. Sheverdyaeva, D. Pacilé, M. Papagno, L. Ferrari, D. Topwal, E. Vescovo, G. Bihlmayer, F. Freimuth, Y. Mokrousov, and S. Blügel, Asymmetric band gaps in a Rashba film system, Phys. Rev. B **93**, 125409 (2016).

[53] G. Géranton, B. Zimmermann, N. H. Long, P. Mavropoulos, S. Blügel, F. Freimuth, and Y. Mokrousov, Nonlocal fieldlike spin-orbit torques in Rashba systems: *Ab initio* study of a Ag_2Bi-terminated Ag(111) film grown on a ferromagnetic Fe(110) substrate, Phys. Rev. B **95**, 134449 (2017).

[54] In view of the similarity of the band structure of the free-standing $BiAg_2$ to paramagnetic BiT_2 (T = Ni, Fe, Co) [20], this situation may be expected to occur also in PbT_2 or BiT_2 surface alloys of the $(\sqrt{3}\times\sqrt{3})R30^\circ$ structure at the (111) surface of ferromagnetic Ni, Fe, or Co.

[55] S. Schulz, I. A. Nechaev, M. Güttler, G. Poelchen, A. Generalov, S. Danzenbächer, A. Chikina, S. Seiro, K. Kliemt, A. Yu. Vyazovskaya, T. K. Kim, P. Dudin, E. V. Chulkov, C. Laubschat, E. E. Krasovskii, C. Geibel, C. Krellner, K. Kummer, and D. V. Vyalikh, Emerging 2D-ferromagnetism and strong spin-orbit coupling at the surface of valence-fluctuating $EuIr_2Si_2$, npj Quantum Mater. **4**, 26 (2019).

[56] O. Krupin, G. Bihlmayer, K. Starke, S. Gorovikov, J. E. Prieto, K. Döbrich, S. Blügel, and G. Kaindl, Rashba effect at magnetic metal surfaces, Phys. Rev. B **71**, 201403(R) (2005).

[57] The behavior of S_z depends on the surface-alloy geometry. For example, an additional study of $BiAg_2$ with the buckling $\Delta z = 0.65$ Å and $\Delta z = 0$ Å (a flat surface-alloy layer) has shown that the out-of-plane spin polarization turns into the ordinary Zeeman spin splitting upon reducing the buckling.